JOURNAL OF GEOPHYSICAL RESEARCH, VOL. 104, NO. D2, PAGES 2093–2104, JANUARY 27, 1999

Monte Carlo calculations of polarized microwave radiation emerging from cloud structures

Laura Roberti

Dipartimento di Elettronica, Politecnico di Torino, Torino, Italy

Christian Kummerow

Laboratory for Atmospheres, NASA Goddard Space Flight Center, Greenbelt, Maryland

Abstract. The last decade has seen tremendous growth in cloud dynamical and microphysical models that are able to simulate storms and storm systems with very high spatial resolution, typically of the order of a few kilometers. The fairly realistic distributions of cloud and hydrometeor properties that these models generate has, in turn, led to a renewed interest in the three-dimensional microwave radiative transfer modeling needed to understand the effect of cloud and rainfall inhomogeneities upon microwave observations. Monte Carlo methods and particularly backward Monte Carlo methods have shown themselves to be very desirable because of the quick convergence of the solutions. Unfortunately, backward Monte Carlo methods are not well suited to treat polarized radiation. This study reviews existing Monte Carlo methods and presents a new polarized Monte Carlo radiative transfer code. The code is based on a forward scheme but uses biasing techniques to keep the computational requirements equivalent to the backward solution. Radiative transfer computations have been performed using a microphysical-dynamical cloud model, and the results are presented together with the algorithm description.

1. Introduction

Passive microwave remote sensing of rainfall has always been hampered by nonlinear relations between rainfall rates and satellite-observed radiances. Nearly 20 years ago, *Weinman and Davies* [1977] and then later *Kummerow and Weinman* [1988a] built radiative transfer models to account for the three-dimensional (3-D) nature of precipitation. Unfortunately, these early models were limited to simple cuboidal geometries, and much of the 3-D effect was determined by the assumptions regarding the size and shape of the clouds. More recently, cloud dynamical models such as those of *Tao et al*. [1987] or *Tripoli* [1992] have made great strides in generating fine-scale cloud and storm properties which appear quite realistic when compared to ground-based radars. Because the cloud models fully specify the atmospheric structure and hydrometeor contents of the storms, these models offer the next level of realism needed to understand the radiative effects of 3-D cloud and rainfall fields.

From a remote sensing point of view the idea of using backward Monte Carlo simulations to deal with these new complex cloud structures in the microwave regime was due to *Petty* [1994], although that paper still dealt with abstract cloud structures. The work was quickly followed by that of *Roberti et al*. [1994], dealing explicitly with cloud dynamical model output, and followed soon thereafter by the work of *Liu et al*. [1996], who first considered polarized radiative transfer, although only in a limited sense. Backward Monte Carlo methods were found to be very easy to implement, flexible, and they allowed an easy interpretation of the interactions of the radiation with the medium. Large absorption cross sections meant that photons were absorbed quickly in the microwave regime leading to numerical convergence with relatively few photons. With solution speeds comparable to analytical approaches, backward Monte Carlo methods are, indeed, attractive because of their simplicity.

One shortcoming of the backward Monte Carlo solutions is their inability to deal properly with polarization introduced by atmospheric constituents unless the vertical and horizontal extinction cross sections are identical, as explained in section 3. Current satellite sensors such as the special sensor microwave imager (SSM/I) and the Tropical Rainfall Measuring Mission microwave imager measure microwave brightness temperature (T_B) in both the horizontal as well as the vertical polarization. Over water backgrounds, emissivities are significantly different for these polarizations, and the T_B differences may thus be used as a measure of the total attenuation of the microwave signal as it propagates through the cloud. Land surfaces generally produce only very small polarization signatures. These signatures are almost impossible to detect in the presence of rainfall which further attenuates any surface signal. An analysis by *Heymsfield and Fulton* [1994], however, revealed 85 GHz polarization signals (ΔT_{V-H}) of about 8–13K over the stratiform precipitation region of both extratropical and tropical mesoscale convective systems (MCS) over land. There is a similar (even if not recurring) pattern at 37 GHz, although the magnitude of the polarization signal does not appear to exceed 7K. No polarization signals were found in the convective portions of these storms. Heymsfield and Fulton argue that these polarization signals cannot be attributed to the surface conditions but must be attributed to atmospheric constituents, and they speculate that they are probably due to nonspherical hydrometeors, such as smaller ice crystals, falling slowly with an

Paper number 1998JD200038.
0148-0227/99/1998JD200038$09.00

approximate horizontal orientation in the less turbulent mesoscale updraft. The lower polarization differences in the convective region could be caused by the presence of randomly oriented snow particles, due to the convective motion, and to the presence of bigger, almost spherical graupel particles.

Backward Monte Carlo schemes cannot, by design, deal with photons changing polarization state. The main reason is that in a backward scheme the first collision is effectively the last collision in the temporal sequence. This implies that when a photon is started, the initial polarization state is unknown. To overcome this problem, *Liu et al*. [1996] developed the so-called "backward-forward" scheme. This scheme does allow for the treatment of polarized radiation but requires that the extinction matrix be diagonal. Observational evidence such as the *Heymsfield and Fulton* [1994] study, which suggests preferentially oriented particles, cannot be dealt with using diagonal extinction matrices. The next development step for microwave radiative transfer codes must be fully polarized 3-D methods. With this aim a new forward Monte Carlo method has been

developed for the solution of the vector radiative transfer equation (VRTE), that is, for the full treatment of the Stokes parameters, when nonspherical oriented hydrometeors are involved.

In the process of obtaining an efficient forward Monte Carlo code, four different Monte Carlo methods have been developed and are described in sections 3–6: (1) a 3-D backward-forward polarized code for spherical or randomly oriented hydrometeors similar to that of *Liu et al*. [1996]; (2) a direct plane-parallel nonpolarized code; (3) a direct plane-parallel polarized code for spherically or randomly oriented spheroidal particles; and (4) a direct plane-parallel polarized code for oriented spheroidal particles. Section 6.3 examines the necessary extensions to make the fully polarized version work within a 3-D framework. The aim of these codes is to simulate the radiance that could be measured by a space-borne radiometer at the top of the atmosphere in a specific direction needed to build a quantitative understanding of the effect of nonspherical particles upon the polarization signatures. The Goddard cumulus ensemble model [*Tao et al*., 1987] serves as a realistic hydrometeor field which can be used to study the behavior for varied hydrometeor shape and density assumptions.

2. Cloud Model and the Computation of Scattering Parameters

All the radiative transfer computations in this study refer to realistic cloud profiles obtained from the cloud microphysical-dynamical model developed by *Tao et al*. [1987]. The cloud domain consists of 64×64 pixels at 15 min in the evolution of the simulated storm. A single time has been chosen which represents a mature squall line. The top boundary is considered as cosmic background with a temperature of $T_c = 2.7$K, while the surface has been assumed to be Lambertian with a temperature of 300K and emissivity $\varepsilon_s = \varepsilon_h = \varepsilon_v = 0.9$. Each pixel consists of 21 vertical layers from the surface to a height of 18 km. The cloud model specifies the height, pressure, temperature, and relative humidity of each layer. Within each layer, cloud water, rain water, cloud ice, snow, and graupel contents are specified. Graupel is assumed to be spherical, and its density is 0.4 g cm^{-3}. Both rain and snow are assumed to be horizontally oriented oblate spheroids. The asymmetry factor a/b for rain, that is, the ratio between the minor and major of the ellipsoids semiaxis, is the same one used by *Kummerow and Weinman* [1988b], and its density is 1 g cm^{-3}. A Marshall and Palmer size distribution is used for snow, rain, and graupel. Two different methods have been used for the computation of the scattering parameters. The first is the T matrix method [*Barber and Hill*, 1990], while the second is the discrete dipole approximation (DDA) [*Draine and Flatau*, 1988]. The codes by *Barber and Hill* [1990] allow the computation of the scattering matrix only for randomly oriented particles, but for the considered cases these codes were faster and more accurate than the DDA codes. It is reasonable to suppose that the polarization differences are mainly due to the different scattering and absorption coefficients, and therefore the matrices for randomly oriented particles have been used also when oriented particles are considered. The obtained results could be slightly altered by this simplification, but the physical considerations are still valid. For spheroidal oriented particles the extinction coefficient and the single scattering albedo have been computed with the T matrix method both for the vertical and horizontal polarization for 30 different polar directions of incidence between 0° and 90°. The particle symmetry allows no computations to be done for different azimuth directions. Mie theory was used for spherical particles.

3. Polarized 3-D Backward-Forward Monte Carlo Method for Spherically or Randomly Oriented Hydrometeors

A backward 3-D Monte Carlo method previously developed by *Roberti et al*. [1994] has been extended to allow the computation of polarized radiation, that is, to solve the VRTE (more details on this subject can be found in the appendix). A similar Monte Carlo method has been developed by *Liu et al*. [1996], while a 3-D discrete ordinate method is described by *Haferman et al*. [1997]. In particular, here and in the following, we adopt the notation of *Chandrasekhar* [1960] describing a beam of polarized radiation with the Stokes parameters $\mathbf{I} = (I_v, I_h, U, V)$, where v and h refer to two mutually orthogonal directions perpendicular and parallel, respectively, to the reference plane. In our case the reference plane is the XY plane. The photons are released at the point of each subcloud where the T_B is to be computed, with the direction opposite to the one in which they would physically propagate. At each scattering event the position of the photon as well as the incident and scattering directions are recorded. When the photon is finally absorbed, then the initial Stokes parameters are $\mathbf{I}_0 = (T_x, T_x, 0, 0)$, where T_x is the physical temperature of the medium at the point of absorption. This assumption can be made because the Planck function is virtually linear with temperature in the microwave regime for typical atmospheric temperatures and can therefore be replaced by T_x. This further implies that the radiances can be interpreted as brightness temperatures rather than power per unit area. Then the path of the photon is traced forward through the scattering events, and the scattering matrix is computed at each step. The Stokes vector after a scattering event is obtained from the Stokes vector before the scattering (primed variables) with the transformation [*Chandrasekhar*, 1960, p. 39]

$$\mathbf{I} = \mathbf{L}(-i_2)\mathbf{T}\mathbf{P}(\cos\theta)\mathbf{T}^{-1}\mathbf{L}(-i_1)/P_{11}\mathbf{I}' = \mathbf{S}\mathbf{I}' \qquad (1)$$

where

Table 1. Comparison of Polarized Brightness Temperatures for the Cloud Model Over Calm Water Presented by *Weinman and Guetter* [1977] at 37 GHz for Different Cosines of Polar Viewing Angle η_v and for Different Rain Rates R

	Stokes Parameter	R = 1 mm/hr	R = 4 mm/hr	R = 16 mm/hr
η_v = 0.23862	I_h	255.5 (253.8)	241.1 (240.0)	222.5 (223.6)
	I_v	235.4 (235.8)	238.0 (237.0)	218.5 (220.2)
η_v = 0.66121	I_h	230.7 (230.7)	252.9 (251.7)	234.4 (235.4)
	I_v	201.3 (200.6)	247.0 (247.3)	232.0 (232.4)
η_v = 0.93247	I_h	204.6 (203.7)	249.2 (248.4)	237.6 (238.6)
	I_v	196.3 (196.0)	247.1 (246.8)	237.2 (237.9)

Values in parentheses are from *Weinman and Guetter* [1977]. Subscripts h and v refer to parallel and perpendicular orthogonal directions.

$$\mathbf{L}(-i) = \begin{pmatrix} \cos^2 i & \sin^2 i & -1/2 \sin 2i & 0 \\ \sin^2 i & \cos^2 i & 1/2 \sin 2i & 0 \\ \sin 2i & -\sin 2i & \cos 2i & 0 \\ 0 & 0 & 0 & 1 \end{pmatrix} \tag{2}$$

$$\mathbf{T} = \begin{pmatrix} 1 & 1 & 0 & 0 \\ 1 & -1 & 0 & 0 \\ 0 & 0 & 1 & 0 \\ 0 & 0 & 0 & 1 \end{pmatrix} \tag{3}$$

$$\mathbf{P} = \begin{pmatrix} P_{11} & P_{12} & 0 & 0 \\ P_{12} & P_{22} & 0 & 0 \\ 0 & 0 & P_{33} & P_{34} \\ 0 & 0 & -P_{34} & P_{44} \end{pmatrix} \tag{4}$$

The scattering matrix **P** coincides with the definition given by *van de Hulst* [1957, p. 44]. In particular, P_{11} is the phase function for the unpolarized radiation. The division by P_{11} in (1) is necessary to remove the bias introduced by the biased sampling of direction after scattering. In fact, $\eta = \cos \vartheta$ is sampled from P_{11}, and i_1 is sampled randomly between 0 and 2π, which are only a first approximation of the correct distributions [*Kattawar and Plass*, 1968; *Collins et al*., 1972]. The angle i_2 can computed from trigonometry [*Liou*, 1980, p. 223]. The final Stokes vector is finally derived as

$$\mathbf{I} = \mathbf{S}_N \cdots \mathbf{S}_1 \mathbf{I}_0 \tag{5}$$

where N is the number of scattering events. The surface can be either specular or Lambertian with a given angular and polarization dependent emissivity. If an interaction with the surface occurs, a random number r uniformly distributed between [0, 1] is compared with both the vertical and horizontal emissivities ε_h and ε_v. Three different events may occur.

If

$$r \le \varepsilon_h \qquad r \le \varepsilon_v \tag{6}$$

then the photon is absorbed and the corresponding Stokes vector is $\mathbf{I}_0 = (T_s, T_s, 0, 0)$, where T_s is the surface temperature. If

$$r > \varepsilon_h \qquad r > \varepsilon_v \tag{7}$$

then the photon is scattered; otherwise if

$$r \le \varepsilon_h \qquad r > \varepsilon_v \tag{8}$$

then the photon is scattered and traced through the successive scattering events until it is finally absorbed with $\mathbf{I}_0 = (T_x, 0, 0, 0)$. Then the scattering events are traced forward, and the Stokes vector is multiplied by the appropriate scattering matrices as in (1) until the interaction with the surface occurs. At that point the surface temperature T_S is added to the I_h component of the current Stokes vector. If the surface is Lambertian, the scattering matrix is given by

$$\mathbf{TP}(\cos \theta)\mathbf{T}^{-1} = \frac{\cos \theta}{\pi} \begin{pmatrix} 0.5 & 0.5 & 0 & 0 \\ 0.5 & 0.5 & 0 & 0 \\ 0 & 0 & 0 & 0 \\ 0 & 0 & 0 & 0 \end{pmatrix} \tag{9}$$

An analog procedure is followed if $r > \varepsilon_h$ and $r \le \varepsilon_v$. To test the validity of the code, the results have been compared with those given by *Weinman and Guetter* [1977] for a plane parallel cloud, and they have been found to be in good agreement. In Table 1 some results of the comparison at 37 GHz are presented for the cloud model over calm water described by *Weinman and Guetter* [1977] for different cosines of the polar viewing angle and different rain rates.

In summary, this backward-forward polarized code can successfully take into account spherical or randomly oriented spheroidal particles, in which cases the extinction and scattering parameters are equal for the two polarizations. Only the surface emissivity can be different for the two polarizations. The code can take into account horizontal as well as vertical inhomogeneities of the medium.

4. Nonpolarized Direct Monte Carlo Method

To correct for the inability of backward Monte Carlo or even backward-forward methods to deal with nondiagonal scattering matrices the development of a polarized forward Monte Carlo method is required. The first step was to develop a nonpolarized forward Monte Carlo code competitive in terms of speed of convergence with the backward Monte Carlo code developed by *Roberti et al*. [1994]. For this and the following codes the medium is considered to be plane parallel, even if the method could be extended in a future work, to consider the horizontal inhomogeneities of the cloud as suggested in section 6.3. With a forward Monte Carlo method the photons are released by the medium coherently with the source parameters, and their propagation is followed until the escape from the medium. Unfortunately, to simulate the T_B that could be measured by a spaceborne radiometer, only the photons which escape the medium in a specific point and direction will be taken into account. This usually involves high computational times because only a fraction of the photons contribute to the

radiance. To overcome this problem, a number of biasing techniques [see also *Roberti*, 1997] are used.

4.1. Source Parameters

The first problem in the definition of the source concerns the choice between the atmosphere, the surface, or the cosmic background as an emission source and has been solved by computing the irradiance which is proportional to the number of photons emitted. The total irradiance for a plane-parallel atmosphere of height Z_0 is equal to

$$F_a = \int_0^{z_0} \int_{4\pi} \varepsilon(z)T(z)k(z)\, d\Omega\, dz$$

$$= 4\pi \int_0^{z_0} \varepsilon(z)T(z)k(z)\, dz \tag{10}$$

where ε, T, k are the emissivity, the physical temperature, and the extinction coefficient, respectively, at height z. The irradiance of a Lambertian surface is equal to

$$F_S = \int_{2\pi} \varepsilon_S T_s \cos\,\theta\, d\Omega = \pi \varepsilon_S T_S \tag{11}$$

where ε_S and T_S represent the surface emissivity and temperature, respectively. The irradiance of the cosmic background of temperature, $T_c = 2.7$K is equal to

$$F_c = \pi T_c \tag{12}$$

The photon is released from the atmosphere if

$$r < F_a/(F_a + F_S + F_c) \tag{13}$$

and is released in a similar manner for the other sources. In the atmosphere a uniform emission in the vertical direction has been chosen. The direction of emission will be isotropic for the atmosphere and Lambertian for the surface.

4.2. Tracing Procedure

The distance to collision is computed using two different methods depending on whether the photon is down-welling or upwelling. If the photon extended path intersects the surface, the optical distance to collision τ_{coll} is computed as

$$\tau_{\text{coll}} = -\ln\,(r) \tag{14}$$

where r is a random number uniformly distributed between [0, 1]. If the photon extended path intersects the upper boundary of the atmosphere, a collision is forced before the photon escapes the medium by selecting the optical distance from the truncated exponential distribution [*Collins et al*., 1982] so that

$$\tau_{\text{coll}} = -\ln\,[1 - r(1 - e^{-\tau_i})] \tag{15}$$

where τ_i is the optical distance along the photon path from the current photon position to the upper boundary of the atmosphere. In this case the photon weight is adjusted by multiplying it by the factor

$$(1 - e^{-\tau_i}) \tag{16}$$

After computing the distance to collision, the photon can find itself in two possible situations: (1) If the photon crosses a boundary before interacting with the medium, it is advanced to the boundary, and a new distance to collision is computed taking into consideration the distance already traveled [*House and Avery*, 1969]. The photon is then relaunched from the boundary it would have crossed. (2) If a collision occurs, then a scattering event is forced thus avoiding absorption. The corresponding bias is removed by multiplying the photon weight by the single scattering albedo $\Lambda(z)$ of the medium in the current position of the photon, which represents the probability of photon survival. If the collision is with the surface, the photon weight is multiplied by $(1 - \varepsilon_S)$. The new direction after scattering is computed using the phase function. Furthermore, to reduce computational times, the contribution that the photon would give to the T_B if scattered in the viewing direction and if propagated to the upper boundary of the atmosphere without any further interaction with the medium is computed, and the photon weight is modified accordingly. In the following, $W_{i,n}$ denotes the weight effectively attached to the nth photon during the propagation at the ith scattering event, and $W'_{i,n}$ indicates the weight attached to the nth photon when its contribution to the T_B if scattered (or emitted) in the viewing direction is computed. The photon weights are modified as follows:

$$\begin{aligned}
W_{0,n} &= 1 \text{ (emission)} & W'_{0,n} &= p(\cos\,\Theta_0)e^{-\tau_0 W_{0,n}} \\
W_{1,n} &= \Lambda_1 W_{0,n} & W'_{1,n} &= p(\cos\,\Theta_1)e^{-\tau_1 W_{1,n}} \\
W_{2,n} &= \Lambda_2 W_{1,n} & W'_{2,n} &= p(\cos\,\Theta_2)e^{-\tau_2 W_{2,n}} \\
W_{i+1,n} &= \Lambda_{i+1} W_{i,n} & W'_{i+1,n} &= p(\cos\,\Theta_{i+1})e^{-\tau_{i+1} W_{i+1,n}}
\end{aligned} \tag{17}$$

where Λ_i is the single scattering albedo at the considered layer and $p(\cos\,\Theta_i)$ is either the atmospheric or the surface phase function, evaluated on the angle between the incidence and the viewing direction, and it gives the probability that the photon is scattered in the viewing direction. The phase function $p(\cos\,\Theta_0)$ for the emission contribution is $1/4\pi$ for the atmosphere and is $\cos\,(\theta_V)/\pi$ for the Lambertian surface, where θ_v is the polar viewing angle. Value τ_i is the optical depth from the point in which the ith collision has occurred to the upper boundary along the viewing direction. Exponent $(-\tau_i)$ in (17) gives the probability that the photon crosses the atmosphere from the point of collision to the top of the atmosphere in the viewing direction without undergoing any other collision with the medium. The photon continues to propagate until the associated weight becomes less than the threshold below which the photon is eliminated. The threshold value has been fixed at 10E^{-6} in all the computations that follow. In the present approach, photon weights are always multiplied by quantities lower than one so that the convergence is assured.

4.3. T_B Computation

The irradiance emitted by the atmosphere is computed as the sum of the contributions of all the layers of infinitesimal thickness dz (equation (10)). With a Monte Carlo method the integral in (10) is computed numerically as

$$F_a = 4\pi \int_0^{z_0} \varepsilon(z)T(z)k(z)\, dz \approx 4\pi \frac{Z_0}{N_a} \sum_{n=1,N_a} \varepsilon_n T_n k_n \tag{18}$$

where N_a is the number of photons emitted by the atmosphere and Z_0 is the atmosphere height. Values ε_n, T_n, and k_n depend on the height of emission z of the nth photon. The fraction $\bar{F}_a$ of F_a which effectively contributes to the T_B is

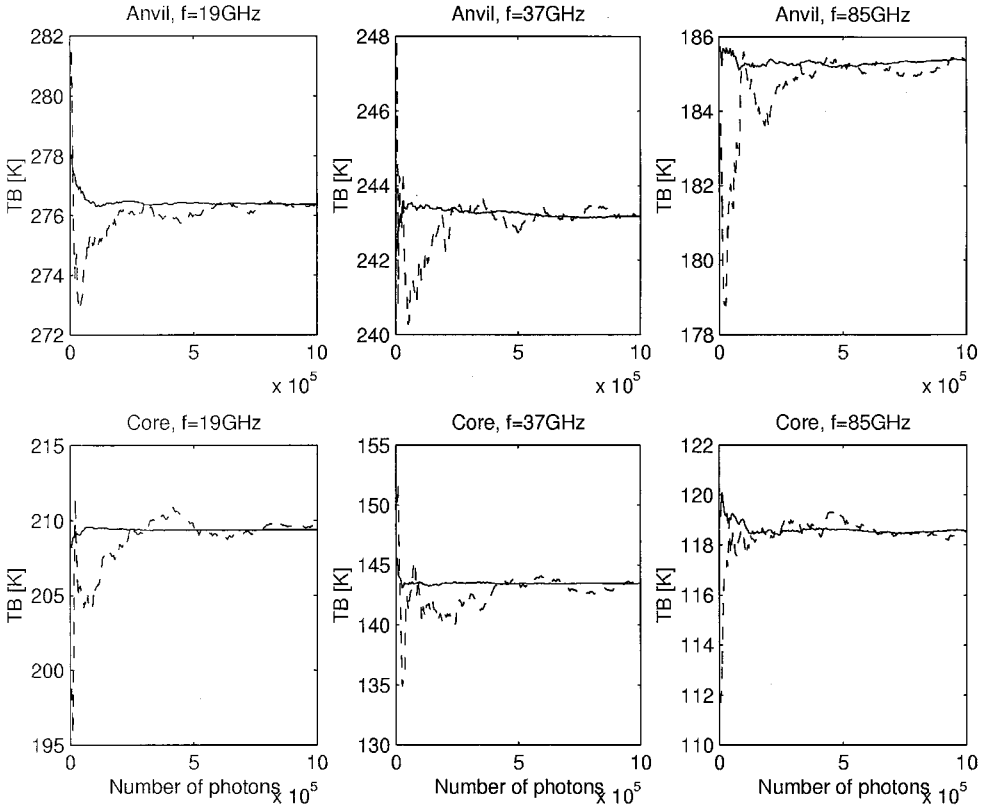

Figure 1. T_B as a function of the number of photons for a subcloud in the anvil region and a subcloud in the core region of the cloud for density of snow 0.1 g/cm^3 for three different frequencies (19.35, 37.0, and 85.6 GHz), obtained with the nonpolarized backward Monte Carlo code (solid curve) and the forward code (dashed curve). Spherical particles are considered. Polar viewing angle $\theta_v = 50°$.

$$\tilde{F}_a = 4\pi \frac{Z_0}{N_a} \sum_{n=1,N_a} \varepsilon_n T_n k_n \sum_{i=0,N} \left(\prod_{j=1,i} \Lambda_j \right) p(\cos\Theta_i) e^{-\tau_i} \, d\Omega_{vi}$$

$$= 4\pi \frac{Z_0}{N_a} \sum_{n=1,N_a} \varepsilon_n T_n k_n \sum_{i=0,N} W'_{i,n} \, d\Omega_{vi} \tag{19}$$

where N is the number of scattering events of the considered photon ($i = 0$ indicates emission), $p(\cos\Theta)e^{-\tau} \, d\Omega_v$ represents the probability that the photon after a scattering event propagates to the upper boundary of the medium in the viewing direction (i.e., in an infinitesimal solid angle $d\Omega_V$) without undergoing any other collision. The atmospheric contribution to the T_B can be computed by dividing $\tilde{F}_a$ by $\cos(\theta_V) \, d\Omega_V$.

$$T_{Ba} \approx \frac{4\pi}{\cos\theta_V} \frac{Z_0}{N_a} \sum_{n=1,N_a} \varepsilon_n T_n k_n \sum_{i=0,N} W'_{i,n} \tag{20}$$

The contribution to the T_B given by the surface emission is

$$T_{BS} \approx \frac{\pi}{\cos\theta_V} \frac{1}{N_S} \sum_{n=1,N_S} \varepsilon_S T_S \sum_{i=0,N} W'_{i,n} \tag{21}$$

where N_S is the number of photons emitted by the surface. The contribution to the T_B given by the cosmic background is

$$T_{Bc} \approx \frac{\pi}{\cos\theta_V} \frac{1}{N_c} \sum_{n=1,N_c} T_c \sum_{i=0,N} W'_{i,n} \tag{22}$$

where N_C is the number of photons emitted by the cosmic background. Consequently, the T_B can be computed as a sum of (20), (21), and (22).

$$T_B = T_{Ba} + T_{Bs} + T_{Bc} \tag{23}$$

The results of this code have been compared with those of an equivalent backward code [*Roberti*, 1997]. In Figure 1 the resulting T_B are presented both for a subcloud in the anvil (stratiform region) and a subcloud in the core (convective region) for three different frequencies. A polar viewing angle $\theta_V = 50°$, similar to the SSM/I one, has been chosen for this simulation and the ones that follow. Spherical particles are considered in this case, and the scattering parameters are computed from Mie theory. The convergence of the forward code (dashed curve) is slower, and the oscillations are higher. Nevertheless, in the worst case, only 500,000 photons are needed to keep the oscillations below 1K.

5. Direct Polarized Monte Carlo Method (Spherically or Randomly Oriented Spheroidal Hydrometeors)

The code described in section 4 has been extended to include the polarization to treat spherically or randomly oriented spheroidal hydrometeors.

5.1. Tracing Procedure

The choice of the photons emission source is based, as for the unpolarized radiation, on the irradiances of the different sources. For spherical or random oriented spheroidal particles the extinction matrix for the Stokes vector is a constant times the unit matrix, which means that the four components of the Stokes vector are subject to the same extinction. Therefore the distance to collision can be computed as for the unpolarized radiation. Also, the single scattering albedos for the horizontal and vertical polarization Λ_h and Λ_v, respectively, are equal. After emission a scattering event is forced at every collision by multiplying the photon weight by the single scattering albedo, and the new direction is determined by sampling the phase function. The new Stokes vector after a collision is computed as in (1). The photon weight vector of the nth photon is modified in a way similar to the unpolarized case (equation (17)), except that the scattering matrix substitutes for the phase function and the matrix $\mathbf{L}$ substitutes for the single scattering albedo (see (25) below)

$$\begin{aligned}
&\mathbf{W}_{0,n} = \mathbf{1} && \mathbf{W}'_{p,n} = p(\cos\Theta_0)e^{-\tau_0}\ \mathbf{W}_{0,n}\\
&\mathbf{W}_{1,n} = \tilde{\mathbf{S}}_1\ \mathbf{L}_1\ \mathbf{W}_{0,n} && \mathbf{W}'_{1,n} = e^{-\tau_1}\ \mathbf{S}_1\ \mathbf{L}_1\ \mathbf{W}_{0,n}\\
&\mathbf{W}_{2,n} = \tilde{\mathbf{S}}_2\ \mathbf{L}_2\ \mathbf{W}_{1,n} && \mathbf{W}'_{2,n} = e^{-\tau_2}\ \mathbf{S}_2\ \mathbf{L}_2\ \mathbf{W}_{1,n}\\
&\mathbf{W}_{i+1,n} = \tilde{\mathbf{S}}_{i+1}\ \mathbf{L}_{i+1}\ \mathbf{W}_{i,n} && \mathbf{W}'_{i+1,n} = e^{-\tau_{i+1}}\ \mathbf{S}_{i+1}\ \mathbf{L}_{i+1}\ \mathbf{W}_{i,n}
\end{aligned} \tag{24}$$

The matrices $\tilde{\mathbf{S}}$ in (24) are evaluated on the angle between the photon incidence and the scattering direction, while the matrices $\mathbf{S}$ are evaluated between the incidence and the viewing direction. The expression for matrices $\mathbf{S}$ is given in (1) and

$$\mathbf{L} = \mathrm{diag}\left(\Lambda_v,\ \Lambda_h,\ \frac{\Lambda_h + \Lambda_v}{2},\ \frac{\Lambda_h + \Lambda_v}{2}\right) \tag{25}$$

The photon continues the propagation until the first two components of the Stokes vector become lower than a fixed threshold and the photon is eliminated.

5.2. Computation of the Stokes Vector

As for the unpolarized radiation, the contribution to the final Stokes vector given by photons emitted by the atmosphere and the surface (cosmic background) is

$$\mathbf{I}_a \approx \frac{4\pi}{\cos\theta_v}\frac{Z_0}{N_a}\sum_{n=1,N_a}\sum_{i=0N}\mathbf{W}'_{i,n}\begin{pmatrix} k_n\varepsilon_n T_n \\ k_n\varepsilon_n T_n \\ 0 \\ 0 \end{pmatrix} \tag{26}$$

$$\mathbf{I}_{S(c)} \approx \frac{\pi}{\cos\theta_v N_{S(c)}}\sum_{n=1,N_{S(c)}}\sum_{i=0N}\mathbf{W}'_{i,n}\begin{pmatrix} \varepsilon_S T_S(T_c) \\ \varepsilon_S T_S(T_c) \\ 0 \\ 0 \end{pmatrix} \tag{27}$$

respectively. The Stokes vector at any computational point and direction is given by

$$\mathbf{I} = \mathbf{I}_a + \mathbf{I}_S + \mathbf{I}_c \tag{28}$$

Numerical results will be presented in section 6.4.

6. Direct Polarized Monte Carlo Method for Oriented Spheroidal Particles

Applying a backward or even a backward-forward Monte Carlo scheme when oriented spheroidal particles are involved gives rise to a number of problems. The values of the single scattering albedos, being dependent on the direction of incidence, are such that the probability of scattering is different depending on the photon propagating toward or from the detector. The use of a direct method seems ideal to avoid such problems. Furthermore, the extinction matrix is of the type

$$\mathbf{K}_e(x, y, z, \theta) = \begin{pmatrix} k_v & 0 & 0 & 0 \\ 0 & k_h & 0 & 0 \\ 0 & 0 & \dfrac{k_h + k_v}{2} & k_c \\ 0 & 0 & -k_c & \dfrac{k_h + k_v}{2} \end{pmatrix} \tag{29}$$

and therefore a different extinction coefficient is associated to each Stokes component, and this must be carefully considered in the photon propagation. Since the matrix is not diagonal, the extinction of each Stokes component depends also on the values of other components. A backward method seems to be useless in this respect because the Stokes vector is unknown during the propagation. While fast and exact methods are available for oriented spheroidal particles in a plane-parallel atmosphere [*Czekala*, 1998; *Czekala and Simmer*, 1998], the results from these simulations are included for completeness (section 6.4).

6.1. Source Parameters

The choice of the emission source is made in a way similar to the ones described in section 4.1. For the atmosphere the following quantities, which represent the average number of photons emitted by the atmosphere and the surface, are computed:

$$F_a = (F_{a_h} + F_{a_v})/2 \tag{30}$$

$$F_S = (F_{S_h} + F_{S_v})/2 \tag{31}$$

F_{a_h}, F_{a_v}, F_{S_h}, and F_{S_v} are the same quantities as in (10) and (11) except that the emissivities can be different for the horizontal and vertical polarization. Equation (12) is still valid for the cosmic background. These quantities are necessary for the computation of the unknown Stokes vector. To increase the speed of convergence, it is useful to employ quantities which represent the real proportion between the energy emitted by the different sources. In the following the extinction matrix will be considered as diagonal, neglecting the circular polarization term, and the error introduced by this approximation should be negligible (see the appendix). To overcome the problem of different extinction coefficients for the different components of the Stokes vector, another biasing technique is introduced, sampling the distance to collision from a biased probability distribution and multiplying the Stokes vector by proper coefficients to remove the statistical perturbation introduced. For down-welling photons the biased probability density for the optical distance to collision is

$$\tilde{p}(\tau)\ d\tau = e^{-\tilde{k}x}\ d(\tilde{k}x) \tag{32}$$

where $\tilde{k}$ is an extinction coefficient computed as

$$\tilde{k} = \frac{1}{\ln\left(\dfrac{2}{e^{-1/k_h} + e^{-1/k_v}}\right)} \tag{33}$$

where k_h and k_v are the extinction coefficients for the two polarizations. This choice has been made in order to minimize the multiplying factors for the elimination of the bias. The distance to collision is given by

$$d_{\text{coll}} = -(1/\tilde{k})\ \ln\ (r) \tag{34}$$

and the matrix for the correction of the bias is given by

$$\tilde{\mathbf{W}}_d = \begin{pmatrix} \dfrac{k_v}{\tilde{k}}\dfrac{e^{-k_v d_{\text{coll}}}}{e^{-\tilde{k} d_{\text{coll}}}} & 0 & 0 & 0 \\ 0 & \dfrac{k_h}{\tilde{k}}\dfrac{e^{-k_h d_{\text{coll}}}}{e^{-\tilde{k} d_{\text{coll}}}} & 0 & 0 \\ 0 & 0 & \dfrac{(k_h+k_v)}{2\tilde{k}}\dfrac{e^{-(k_h+k_v)d_{\text{coll}}/2}}{e^{-\tilde{k} d_{\text{coll}}}} & 0 \\ 0 & 0 & 0 & \dfrac{(k_h+k_v)}{2\tilde{k}}\dfrac{e^{-(k_h+k_v)d_{\text{coll}}/2}}{e^{-\tilde{k} d_{\text{coll}}}} \end{pmatrix} \tag{35}$$

where the diagonal elements represent the ratio between the real and the biased probability. For upwelling photons, as explained in section 4.2, a collision is forced before photons escape the medium, and the distance to collision becomes

$$d_{\text{coll}} = -(1/\tilde{k})\ \ln\ [1 - r(1 - e^{-\tilde{\tau}})] \tag{36}$$

where $\tilde{\tau}$ is the optical thickness computed from the current photon position to the top of the atmosphere in the direction of propagation using the extinction coefficient $\tilde{k}$ in (33). The weight correction matrix is similar to the one in (35), except that each element is still multiplied by a factor $(1 - e^{-\tilde{\tau}})$. Some attention must be paid to the computation of the new distance to collision after the crossing of an internal boundary of the medium. The true distance to collision probability densities for a photon crossing the boundary between layer 1 and 2 are

$$\begin{aligned} p_h(\tau)\ d\tau &= e^{-k_{h1}d_1}e^{-k_{h2}(d-d_1)}\ d(k_{h2}d) \qquad d > d_1 \\ p_v(\tau)\ d\tau &= e^{-k_{v1}d_1}e^{-k_{v2}(d-d_1)}\ d(k_{v2}d) \qquad d > d_1 \end{aligned} \tag{37}$$

for the H and V polarized photons, where d_1 is the distance between the current photon position to the boundary in the direction of propagation of the photon. The biased probability density with which the distance to collision inside the new layer is corrected taking into account the distance already traveled is

$$\tilde{p}(\tau)\ d\tau = e^{-\tilde{k}_1 d_1}e^{-\tilde{k}_2(d-d_1)}\ d(\tilde{k}_2 d) \qquad d > d_1 \tag{38}$$

The distance to collision in the second medium becomes

$$d_{\text{coll-new}} = (\tilde{k}_1/\tilde{k}_2)(d_{\text{coll-old}} - d_1) \tag{39}$$

where $d_{\text{coll-old}}$ is the distance to collision computed in the first medium. Therefore the weight correction matrix is a diagonal matrix with elements representing the ratio between the real and the biased probability

$$\begin{aligned} \tilde{\mathbf{W}}_{11} &= C\,\frac{k_{v2}}{\tilde{k}_2}\,\frac{e^{-k_{v1}d_1}e^{-k_{v2}d_{\text{coll-new}}}}{e^{-\tilde{k}_1 d_1}e^{-\tilde{k}_2 d_{\text{coll-new}}}} \\ \tilde{\mathbf{W}}_{22} &= C\,\frac{k_{h2}}{\tilde{k}_2}\,\frac{e^{-k_{h1}d_1}e^{-k_{h2}d_{\text{coll-new}}}}{e^{-\tilde{k}_1 d_1}e^{-\tilde{k}_2 d_{\text{coll-new}}}} \\ \tilde{\mathbf{W}}_{33} &= C\,\frac{k_{h2}+k_{v2}}{2\tilde{k}_2}\,\frac{e^{-[(k_{h1}+k_{v1})/2]d_1}e^{-[(k_{h2}+k_{v2})/2]d_{\text{coll-new}}}}{e^{-\tilde{k}_1 d_1}e^{-\tilde{k}_2 d_{\text{coll-new}}}} \\ \tilde{\mathbf{W}}_{44} &= C\,\frac{k_{h2}+k_{v2}}{2\tilde{k}_2}\,\frac{e^{-[(k_{h1}+k_{v1})/2]d_1}e^{-[(k_{h2}+k_{v2})/2]d_{\text{coll-new}}}}{e^{-\tilde{k}_1 d_1}e^{-\tilde{k}_2 d_{\text{coll-new}}}} \end{aligned} \tag{40}$$

C is equal to $(1 - e^{-\tilde{\tau}})$ for upwelling photons, and $C = 1$ in the opposite case.

6.2. Tracing Procedure

The photon weights during the propagation are modified as follows

$$\begin{aligned} W_0 &= \vec{1} \qquad W_0' = p(\cos\ \Theta_0)\ \ \mathbf{E}_0 W_0 \\ W_1 &= \tilde{\mathbf{S}}_1\ \ \mathbf{K}^{-1}(z_1,\ \theta_0)\ \ \mathbf{K}(z_1,\ \theta_1)\ \ \mathbf{L}(z_1,\ \theta_0) \\ W_1' &= \mathbf{S}_1\ \ \mathbf{K}^{-1}(z_1,\ \theta_0)\ \ \mathbf{K}(z_1,\ \theta_v)\ \ \mathbf{E}_1\ \ \mathbf{W}_0 \\ W_2 &= \tilde{\mathbf{S}}_2\ \ \mathbf{K}^{-1}(z_2,\ \theta_1)\ \ \mathbf{K}(z_2,\ \theta_2)\ \ \mathbf{L}(z_2,\ \theta_1) W_1 \\ W_2' &= \mathbf{S}_2\ \ \mathbf{K}^{-1}(z_2,\ \theta_1)\ \ \mathbf{K}(z_2,\ \theta_v)\ \ \mathbf{E}_2\ \ \mathbf{W}_1 \\ W_{i+1} &= \tilde{\mathbf{S}}_{i+1}\ \ \mathbf{K}^{-1}(z_{i+1},\ \theta_i)\ \ \mathbf{K}(z_{i+1},\ \theta_{i+1})\ \ \mathbf{L}(z_{i+1},\ \theta_i) W_i \\ W_{i+1}' &= \mathbf{S}_{i+1}\ \ \mathbf{K}^{-1}(z_{i+1},\ \theta_i)\ \ \mathbf{K}(z_{i+1},\ \theta_v)\ \ \mathbf{E}_{i+1}\ \ \mathbf{W}_i \end{aligned} \tag{41}$$

where

$$\mathbf{E}_i = \text{diag}(e^{-\tau_{v,i}},\ e^{-\tau_{hi}},\ e^{-\tau_{U,i}},\ e^{-\tau_{V,i}}) \tag{42}$$

diag is diagonal and $\tau(h,\ v,\ U,\ V)$, i are the optical thicknesses from the ith scattering point to the observation point computed with the appropriate extinction coefficient

$$\mathbf{K}(z,\ \theta) = \text{diag}\left(k_v(z,\ \theta),\ k_h(z,\ \theta),\ \frac{k_h(z,\ \theta) + k_v(z,\ \theta)}{2},\ \frac{k_h(z,\ \theta) + k_v(z,\ \theta)}{2}\right) \tag{43}$$

The multiplication by $\mathbf{K}^{-1}$ in (41) is introduced to take into account the angular dependency of the extinction coefficient. Matrix $\mathbf{L}$ is given in (25). The final Stokes vector is computed with formulae analogous to (26)–(28).

6.3. Extension of the Code to the 3-D Case

The main problem in the extension of the forward codes to the 3-D case deals with the treatment of the emission sources. If the horizontal inhomogeneities of the medium are to be taken into account, photons should be released by the different layers of the different subclouds according to the thermal contribution. For each subcloud nx, ny a threshold must be fixed as (see (10), (11), and (12))

$$Trs_{nx,ny} = F_{a_{nx,ny}} + F_{s_{nx,ny}} + F_{c_{nx,ny}} \tag{44}$$

If NXCL and NYCL are the subcloud numbers in the x and y directions, a photon is emitted by subcloud nx and ny if a random number r uniformly distributed between [0, 1] satisfies

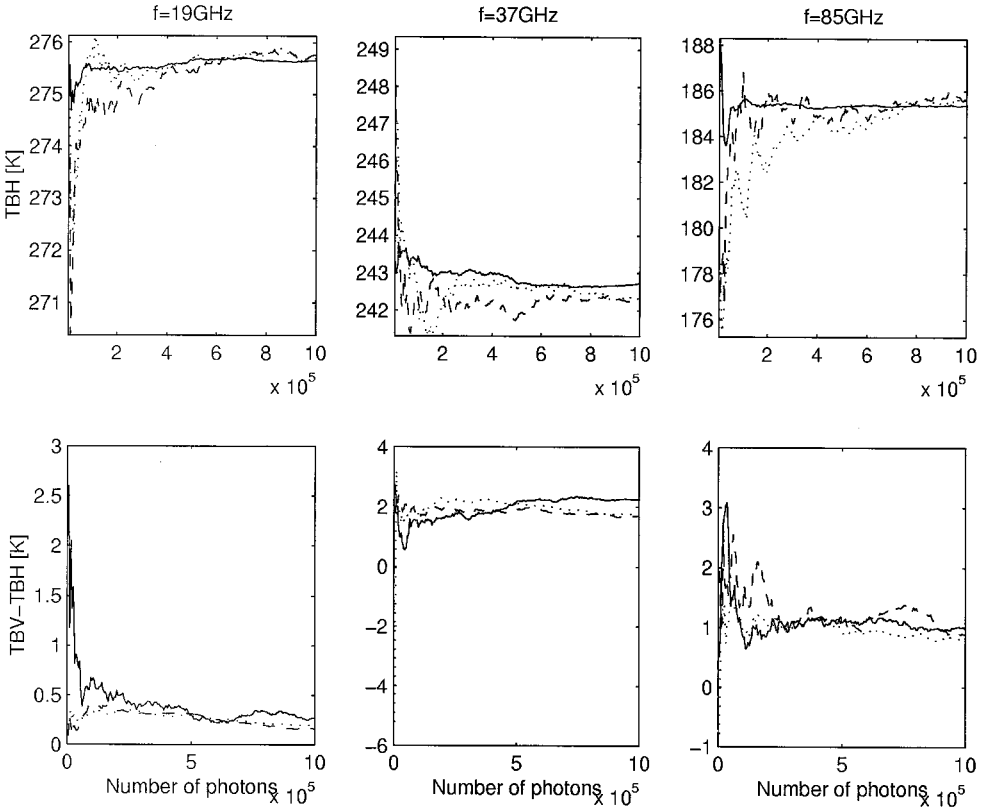

Figure 2. T_H and ΔT_{V-H} as a function of the number of photons for a subcloud in the stratiform region of the cloud for density of snow 0.1 g/cm^3 for three different frequencies (19.35, 37.0, and 85.6 GHz) obtained with the polarized backward-forward Monte Carlo code (solid curve), the forward code for spherical particles (dashed curve), and the forward code for oriented spheroidal particles (dotted curve). Spherical particles are considered. Polar viewing angle $\theta_v = 50°$.

$$\frac{\sum_{j=1,ny-1;\,j=1,\mathrm{NXCL}} Trs_{i,j} + \sum_{j=ny;\,i=1,nx-1} Trs_{i,j}}{\sum_{i=1,\mathrm{NXCL};\,j=1,\mathrm{NYCL}} Trs_{i,j}} < r$$

$$< \frac{\sum_{j=1,ny-1;\,i=1,\mathrm{NXCL}} Trs_{i,j} + \sum_{j=n;y\,i=1,nx} Trs_{i,j}}{\sum_{i=1,\mathrm{NXCL};j=1,\mathrm{NYCL}} Trs_{i,j}} \qquad (45)$$

when the matrix is scanned by lines. Once the subcloud has been determined, the vertical position for emission inside each subcloud can be prescribed as in section 4.1. If the subcloud horizontal dimension is small compared to the vertical dimension, the photons are simply started at the center of the subcloud. Emission points must be sampled uniformly in the case that the subcloud dimension is large compared to the vertical dimension. The computation of the Stokes vector must be partially modified since the Stokes vector must be computed at the top of each subcloud. At each scattering event a line must be ideally drawn from the point of collision to the top of the cloud in the viewing direction. The line will intersect the top of only one of the subclouds. The scattering event will give a contribution only to the Stokes vector associated with that subcloud, and the contribution can be computed as described in section 4.3 for the unpolarized case. The rest of the algorithm remains unchanged. Photons crossing the vertical boundary between two subclouds or the horizontal boundary between two layers are treated analogously to the plane-parallel methods.

6.4. Numerical Results

The convergence of the two forward polarized codes has been analyzed with reference to the backward-forward code. The resulting T_H and ΔT_{V-H} are presented for a subcloud in the stratiform region (Figure 2) for three different frequencies considering spherical hydrometeors. Similar results can be obtained for a subcloud in the convective region. A Lambertian surface with emissivities $\varepsilon_S = \varepsilon_h = \varepsilon_v = 0.9$ has been chosen in order to analyze the polarization signature introduced by atmospheric scattering. The $\vartheta_v = 50°$. Because of the hydrometeors spherical shape, the resulting ΔT_{V-H} are negligible. For nadir observations the ΔT_{V-H} would be zero apart from the numerical oscillations of the Monte Carlo method. The same considerations done for the forward unpolarized code are still valid here. The convergence of the forward codes is slower, but if the required accuracy is of the order of 1K, an average number of 500,000 photons is sufficient.

To simulate the observed polarized results [*Heymsfield and Fulton*, 1994], a cross section of the cloud model, made of 64 subclouds, normal to the main convective line is considered. Both rain and snow are modeled as horizontally oriented spheroids. It might be useful to note here that the observed results revealed 85 GHz polarization signals (ΔT_{V-H}) of about 8–13K over the stratiform precipitation region, while the 37 GHz ΔT_{V-H} did not appear to exceed 7K. Very low polariza-

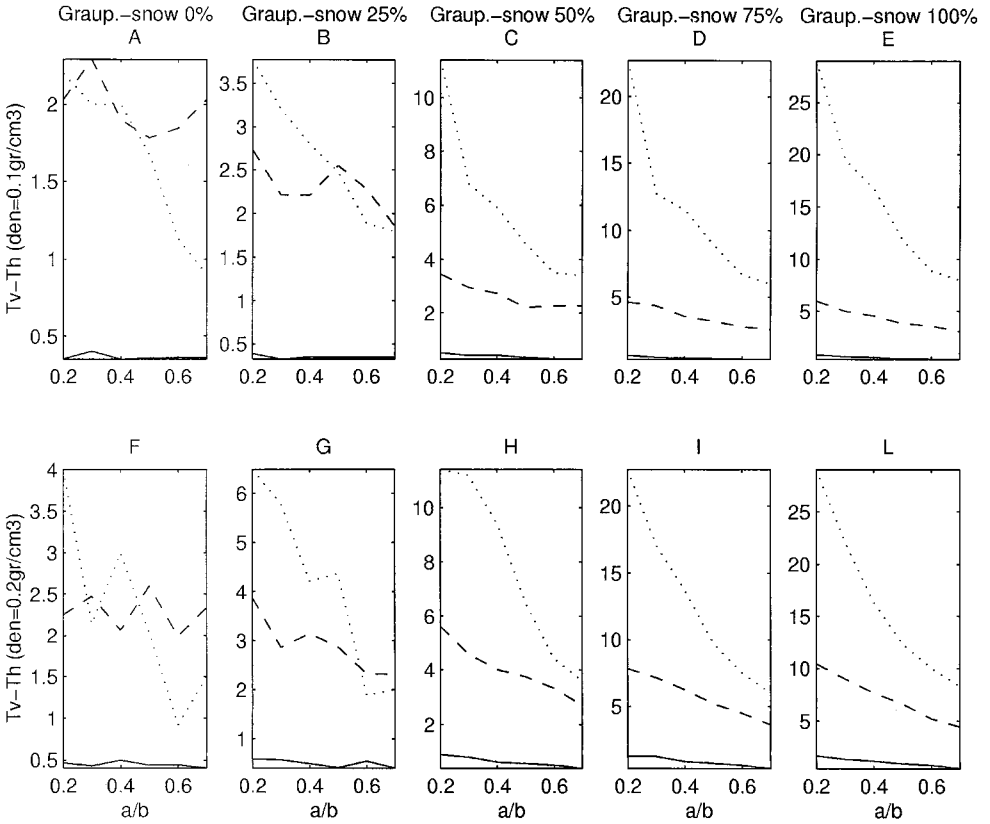

Figure 3. ΔT_{V-H} as a function of the asymmetry factor of horizontally oriented oblate spheroidal particles for a subcloud in the stratiform region of the cloud (density of snow 0.1 and 0.2 g/cm^3 and five percentages of graupel transformed to snow (0, 25, 50, 75, and 100%)). Solid curve is 19.35 GHz, dashed curve is 37.0 GHz, and dotted curve is 85.6 GHz. Polar viewing angle $\theta_v = 50°$.

tion signals were found in the convective portions of these storms. The hypothesis is that the (ΔT_{V-H}) could be attributed to atmospheric constituents, such as smaller ice crystals, falling slowly with an approximate horizontal orientation in the less turbulent mesoscale updraft. The lower polarization differences in the convective region could be caused by the presence of randomly oriented snow particles, due to the convective motion and to the presence of bigger, almost spherical, graupel particles. Therefore, to analyze the effect of horizontally oriented nonspherical snow particles on the polarization signature, a sensitivity analysis of the ΔT_{V-H} as a function of snow density, asymmetry factor (a/b), and concentration using plane-parallel computations on single subclouds is performed. In order to avoid changing the total ice concentration, snow concentration is varied by reducing graupel and keeping the total ice mass constant. The results are presented for a subcloud in the stratiform region (Figure 3) and one in the convective region (Figure 4). The resulting ΔT_{V-H} are shown, as a function of the asymmetry factor, for density of snow equal to 0.1 and 0.2 g/m^3, for five different percentages of graupel transformed to snow (percentage (perc) are 0, 0.25, 0.50, 0.75, and 1.00), and at three frequencies (19, 37, and 85 GHz). In particular, the concentrations of snow and graupel have been computed as

$$\begin{aligned} \text{snow} &= \text{snow} + \text{graupel} \times \text{percentage} \\ \text{graupel} &= \text{graupel} \times (1 - \text{perc}) \end{aligned} \tag{46}$$

As it is reasonable to expect the ΔT_{V-H} increase when the influence of horizontally oriented snow particles is higher, that is, increasing the snow density and the percentage of graupel transformed to snow, that is, the snow concentration. Furthermore, the ΔT_{V-H} are higher when the asymmetry is high (i.e., low-asymmetry factor), and this appears more clearly when the percentage of graupel transformed to snow is more than 50%. If the snow content is low (perc is 0 and 0.25), the ΔT_{V-H} at lower frequencies can be higher than those at 85 GHz. This might be due to the fact that the radiation at 85 GHz is more sensitive to the depolarizing effect of graupel scattering; that is, the presence of bigger spherical particles would have a bigger depolarizing influence at higher frequencies. To obtain the desired ΔT_{V-H} in the anvil, the content of snow originally present in the cloud seems to be too low. It is necessary to transform 50% of the graupel to snow to start obtaining ΔT_{V-H} of 11K at 85 GHz with $\Delta T_{V-H} < 6$K at 37 GHz. This considerations seem to confirm the presence of horizontally oriented nonspherical particles in the stratiform region of MCSs. Conversely, if all the graupel is converted to snow, the ΔT_{V-H} become too high. In the core of the storm, low (perc is 0 and 0.25) or high (perc is 0.75 and 1) snow contents give ΔT_{V-H} which are too low or too high, respectively, with regard to the observed ones. A conversion of 50% of the graupel to snow enables us to simulate realistic polarization differences. This should not be confusing with respect to equivalent conversion in the anvil. In fact, in the core of the cloud the graupel

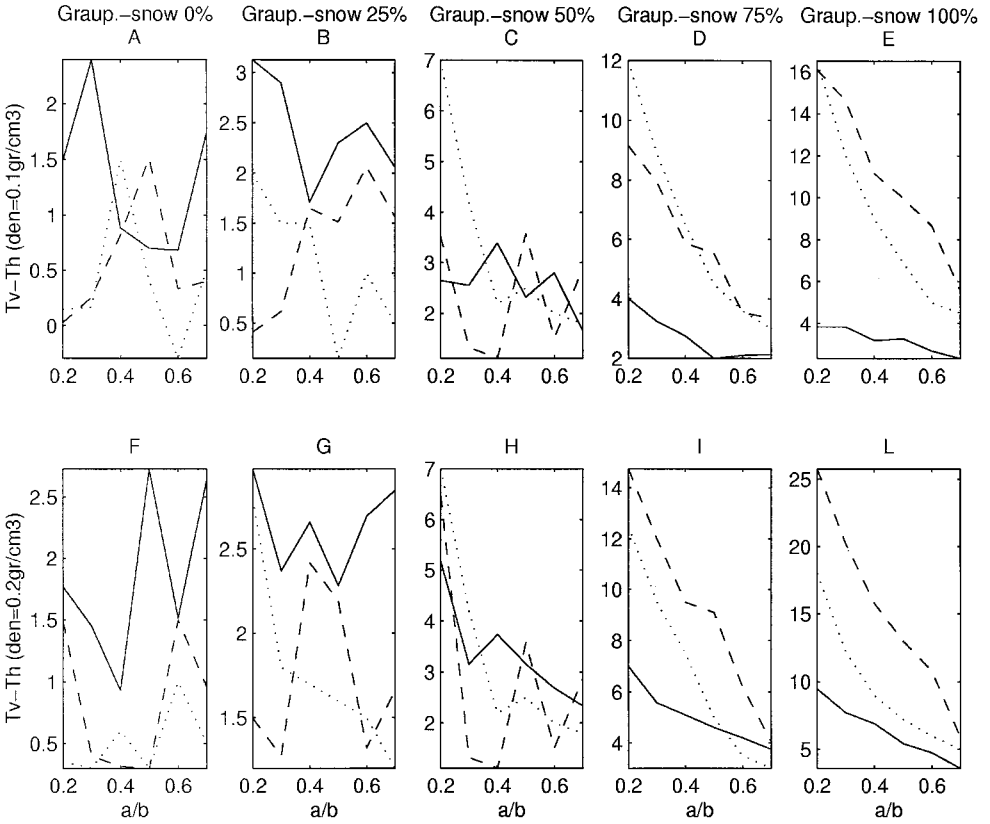

Figure 4. Same as Figure 3 but for a subcloud in the convective region of the cloud.

content is at least 1 order of magnitude higher with respect to the anvil, while the snow content, at least in the lower layers, is comparable. Thus even converting half of the graupel into snow, the remaining graupel content is still much higher than in the stratiform region, and its influence is stronger on the polarization signature. The above considerations may be misleading in the sense that they may lead to the conclusion that in the microphysical-dynamical cloud model used for the simulations (see section 2), the graupel content in the stratiform region is too high with respect to snow. A single observation, as presented in this study, does not allow any conclusions about the accuracy of the cloud model. Nor is this the intent of this analysis. The simulations do demonstrate, however, that is now possible to perform accurate radiative transfer computations through complex cloud structures.

Since the percentage of graupel that, transformed to snow, gives ΔT_{V-H} in accordance with the observed results varies with the different subclouds, we tried to transform graupel to snow, starting from the higher layers of each of the 64 subclouds for a total of 1.5 kg/m^2. This implies that for subclouds in the convective region the snow concentration was modified only in the first few layers on the top; while for some subclouds in the stratiform region, the entire graupel could have been transformed to snow. The resulting T_H and ΔT_{V-H} are shown at 19.37 and 85 GHz in Figures 5a and 5b, respectively. The density of snow is 0.1 g/cm^3; the asymmetry parameter is 0.3. The small negative polarization differences at 37 GHz are due to numerical instabilities of the Monte Carlo code. The obtained results reproduce well the observed ones at all frequencies. The lowest T_B at 85 and 37 GHz, caused by scattering, correspond to the convective region of the cloud where the rain is more intense, and the atmospheric profile is characterized by the presence of bigger ice particles, such as graupel and/or aggregates with no preferential orientation due to the turbulence. The corresponding ΔT_{V-H} are lower than 5K at all frequencies. At both sides of the convective region, where the rain is less intense, emission predominates over scattering and the T_B increase at all frequencies. The ΔT_{V-H} at 85 GHz become higher, and a similar but less noticeable behavior can be observed at 37 GHz.

7. Conclusions

Four different Monte Carlo codes for the computation of microwave radiation emerging from cloud structures have been presented. Three codes allow us to take into account polarization. One of them is 3-D but treats only spherical or randomly oriented hydrometeors which give only a small polarization signal. The code which can deal with oriented spheroidal particles is currently plane-parallel. Future work will concentrate on the extension of this code to the 3-D case. The convergence and accuracy of the forward Monte Carlo codes is lower with respect to backward codes, but computational times are limited thanks to the biasing techniques that have been used. Nevertheless, forward Monte Carlo codes seem to be the only way to treat polarization when oriented nonspherical particles are involved.

One of the forward Monte Carlo codes has been used for a sensitivity analysis of the ΔT_{V-H} as a function of snow parameters. To summarize the results, it is possible to say that while many combinations of density and asymmetry factors can explain the observed ΔT_{V-H}, it was found that converting a total

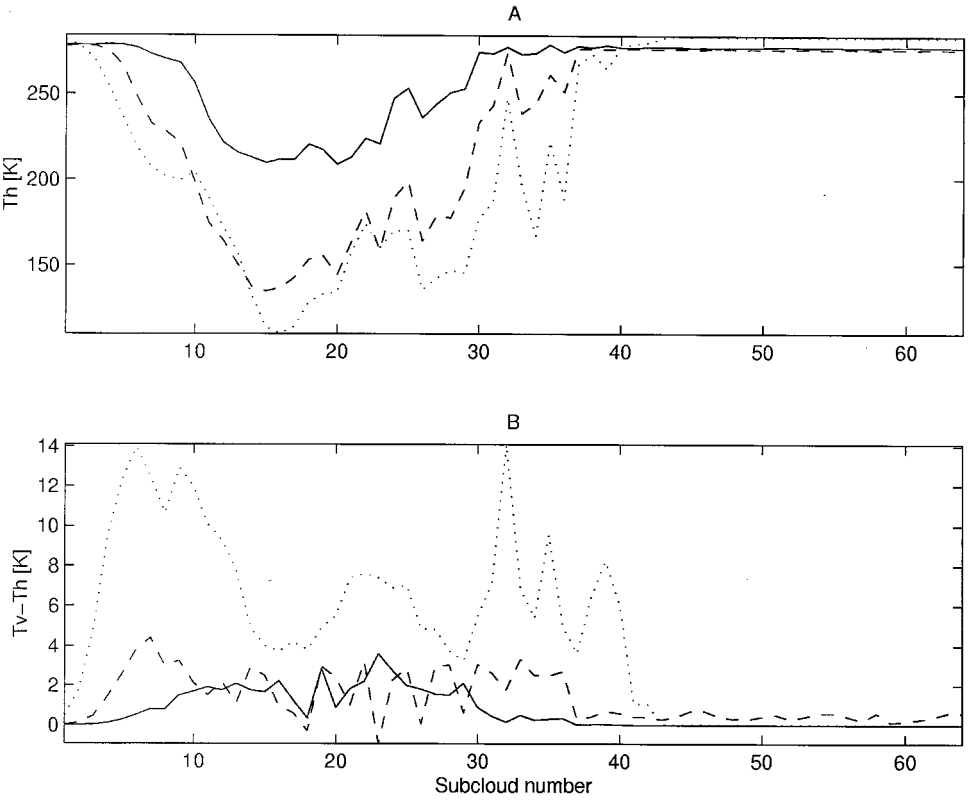

Figure 5. (a) T_H and (b) ΔT_{V-H} associated to the considered cloud section (see section 6.4 for more details). The density of snow is 0.1 g/cm^3; the asymmetry parameter a/b is 0.3. Solid curve is 19.35 GHz, dash curve is 37.0 GHz, and dotted curve is 85.6 GHz. Polar viewing angle $\theta_v = 50°$.

of 1.5 kg/m^2 of graupel into snow throughout the cloud model simulation produced generally adequate agreement with observations. The results represent a contribution to the understanding of cloud microphysics in relation to radiometer observables at millimeter frequencies even if the relatively poor knowledge of the real cloud parameters is underlined. The fact that relatively large adjustments to the graupel and snow concentrations and densities were necessary to replicate the observed polarization signal further implies that such analyses might well lead to verifiable conclusions about cloud structures.

Appendix: Vector Radiative Transfer Equation (VRTE)

In Monte Carlo simulations, as with any radiative transfer solution, the code is complicated significantly when polarized or vector-scattering quantities are required instead of the simpler scalar solutions. The basic polarization signal seen in passive microwave radiometry emanates from smooth ocean surfaces. The reflectivity of these surfaces, while different for H and V polarizations, does not by itself change the polarization state of the photons and therefore does not require a polarized or vector treatment of the radiative transfer solution. The vector solutions are required any time the polarization state of a photon is allowed to change as a consequence of a scattering event. This may be due to nonspherical hydrometeors or preferentially oriented scatterers such as vegetation. In atmospheric applications the effect is typically small (rarely exceeding 20K) but may be important in terms of the information it carries regarding the type and concentration of nonspherical scatterers.

In the radiative transfer theory the polarization of the electromagnetic radiation is described by the Stokes parameters vector $\mathbf{I}(\mathbf{r}, \hat{s}) = (I_h, I_v, U, V)$ which depends on the position $\mathbf{r} = (x, y, z)$ and direction $\hat{s} = (\eta, \phi)$ (for more details on this subject, please refer to *Chandrasekhar* [1960] and *Tsang et al*. [1985]). The VRTE for specific intensity can be obtained using the incoherent addition of Stokes parameters [*Tsang et al*., 1985, p. 127] as

$$\frac{d\mathbf{I}(\mathbf{r}, \hat{s})}{ds} = -\mathbf{k}_e(\mathbf{r}, \hat{s})\mathbf{I}(\mathbf{r}, \hat{s}) + \mathbf{k}_{em}(\mathbf{r}, \hat{s})B + \int_{4\pi} \mathbf{P}(\mathbf{r}, \hat{s}, \hat{s}')\mathbf{I}(\mathbf{r}, \hat{s}')\, d\Omega' \quad \text{(A1)}$$

where $\mathbf{k}_e$ is the extinction matrix which describes the attenuation due to absorption and scattering, $\mathbf{k}_{em}$ is the emissivities vector which, multiplied by the Plank emission function B, gives the thermal emission source, and $\mathbf{P}(\mathbf{r}, \hat{s}, \hat{s}')$ is the phase matrix which characterizes the coupling of intensities in two different directions because of scattering.

For spherical particles the extinction matrix is diagonal and is a constant times the unit matrix. The emission vector has the first two elements equal to each other, and the last two elements are equal to zero. For nonspherical particles the extinction matrix is generally nondiagonal, and the four elements of the emission vector are generally nonzero. For spherical, randomly oriented or spheroidal horizontally oriented particles

the phase matrix is of the type described in (1), (3) and (4). For horizontally oriented spheroidal particles the extinction matrix is of the type in (29). In general, it is difficult to estimate a priori the effect of neglecting the circular polarization term k_c in (29) without performing specific computations [*Mishchenko*, 1994; *Takano and Liou*, 1994]. Nevertheless, the case considered in section 6.3 involves an azimuthally symmetric radiation field since the medium is plane-parallel with thermal sources and the oriented particles are symmetric with random azimuthal orientation. In this case the Stokes components U and V are zero at the emission [*Takano and Liou*, 1993; *Chandrasekhar*, 1960, p. 43]. The V component remains zero also during the photon propagation, while U is not zero because of scattering, but its value is negligible in respect to I_v and I_h. Consequently, the element k_c of the extinction matrix, being a multiplier of the U component, should have a negligible effect on the final Stokes vector.

Acknowledgments. The authors thank W.-K. Tao for providing the three-dimensional microphysical cloud model. Laura Roberti acknowledges partial financial support from the Euro TRMM Project and from CNR/IFA, Rome, Italy.

References

Barber, P. W., and S. C. Hill, *Light Scattering by Particles: Computational Methods*, World Sci., Riveredge, N. J., 1990.

Chandrasekhar, S., *Radiative Transfer*, p. 39, Dover, Mineola, N. Y., 1960.

Collins, D. G., W. G. Blattner, M. B. Wells, and H. G. Horak, Backward Monte Carlo calculations of the polarization characteristics of the radiation emerging from spherical-shell atmospheres, *Appl. Opt*., *11*, 2684–2696, 1972.

Czekala, H., Effects of ice particle shape and orientation on polarized microwave radiation for off-nadir problems, *Geophys. Res. Lett*., *25*, 1669–1672, 1998.

Czekala, H., and C. Simmer, Microwave radiative transfer with nonspherical precipitating hydrometeors, *J. Quant. Spectrosc. Radiat. Transfer*, *60*(3), 365–374, 1998.

Draine, B. T., and P. J. Flatau, Discrete-dipole approximation for scattering calculations, *Astrophys. J*., *333*, 848–872, 1988.

Haferman, J. L., T. F. Smith, and W. F. Krajewski, A multidimensional discrete-ordinates method for polarized radiative transfer, I, Validation for randomly oriented axisymmetric particles, *J. Quant. Spectrosc. Radiat. Transfer*, *58*(3), 379–398, 1997.

Heymsfield, G. M., and R. Fulton, Passive microwave and infrared structure of mesoscale convective systems, *Meteorol. Atmos. Phys*., *54*, 123–139, 1994.

Kattawar, G. W., and G. N. Plass, Radiance and polarization of multiple scattered light from haze and clouds, *Appl. Opt*., *7*, 1519–1528, 1968.

Kummerow, C., and J. A. Weinman, Determining microwave brightness temperatures from precipitating horizontally finite and vertically structured clouds, *J. Geophys. Res*., *93*, 3720–3728, 1988a.

Kummerow, C., and J. A. Weinman, Radiative properties of deformed hydrometeors for commonly used passive microwave frequencies, *IEEE Trans. Geosci. Remote Sens*., *26*, 629–638, 1988b.

Liou, K.-N., *An Introduction to Atmospheric Radiation*, 223 pp., Academic, San Diego, Calif., 1980.

Liu, Q., C. Simmer, and E. Ruprecht, 3-D radiation transfer effects of clouds in the microwave spectral range, *J. Geophys. Res*., *101*, 4289–4298, 1996.

Mishchenko, M. I., Transfer of polarized infrared radiation in optically anisotropic media: Application to horizontally oriented ice crystals: comment, *J. Opt. Soc. Am. A Opt. Image Sci*., *4*, 1376–1377, 1994.

Petty, G. W., Physical retrievals of over-ocean rain rate from multichannel microwave imagery, I, Theoretical characteristics of normalized polarization and scattering indexes, *Meteorol. Atmos. Phys*., *54*, 79–99, 1994.

Roberti, L., Monte Carlo radiative transfer in the microwave and in the visible: Biasing techniques, *Appl. Opt*., *36*, 7929–7938, 1997.

Roberti, L., J. Haferman, and K. Kummerow, Microwave radiative transfer through horizontally inhomogeneous precipitating clouds, *J. Geophys. Res*., *99*, 16,707–16,718, 1994.

Takano, Y., and K. N. Liou, Transfer of polarized infrared radiation in optically anisotropic media: Application to horizontally oriented ice crystals, *J. Opt. Soc. Am. A Opt. Image Sci*., *10*, 1243–1256, 1993.

Takano, Y., and K. N. Liou, Transfer of polarized infrared radiation in optically anisotropic media: Application to horizontally oriented ice crystals: Reply to comment, *J. Opt. Soc. Am. A Opt. Image Sci*., *4*, 1378, 1994.

Tao, K., J. Simpson, and S.-T. Soong, Statistical properties of a cloud ensemble: A numerical study, *J. Atmos. Sci*., *44*, 3175–3187, 1987.

Tripoli, G. J., A non hydrostatic model designed to simulate scale interactions, *Mon. Weather Rev*., *120*, 1342–1359, 1992.

Tsang, L., J. A. Kong, and T. T. Shin, *Theory of Microwave Remote Sensing*, pp. 120–208, John Wiley, New York, 1985.

van de Hulst, H. C., *Light Scattering by Small Particles*, pp. 44, Dover, Mineola, N. Y., 1957.

Weinman, J. A., and R. Davis, Thermal microwave radiances from horizontally finite clouds of hydrometeors, *J. Geophys. Res*., *83*, 3099–3107, 1978.

Weinman, J. A., and P. J. Guetter, Determination of rainfall distributions from microwave radiation measured by the Nimbus 6 ESMR, *J. Appl. Meteorol*., *16*, 437–442, 1977.

C. Kummerow, Laboratory for Atmospheres, NASA Goddard Space Flight Center, Greenbelt, MD 20771. (kummerow@agnes.gsfc.nasa.gov)

L. Roberti, Dipartimento di Elettronica, Politecnico di Torino, Corso Duca degli Abruzzi 24, 10129 Torino, Italy. (roberti@polito.it)

(Received April 22, 1998; revised September 15, 1998;
accepted September 24, 1998.)